Applied Catalysis B: Environmental 300 (2022) 120730

Contents lists available at ScienceDirect

Applied Catalysis B: Environmental

journal homepage: www.elsevier.com/locate/apcatb

Ru(III) single site solid micellar catalyst for selective aqueous phase hydrogenation of carbonyl groups in biomass-derived compounds

Qiyan Wang [a,b,d], Sara Santos [c,d,1], César A. Urbina-Blanco [c,d], Wenjuan Zhou [b,d], Yong Yang [d,e], Maya Marinova [d,f], Svetlana Heyte [a,d], Thuriot-Roukos Joelle [a,d], Ovidiu Ersen [d,g], Walid Baaziz [d,g], Olga V. Safonova [d,h], Mark Saeys [c,d], Vitaly V. Ordomsky [a,d]

[a] Univ. Lille, CNRS, Centrale Lille, ENSCL, Univ. Artois, UMR 8181 – UCCS – Unité de Catalyse et Chimie du Solide, F-59000 Lille, France
[b] Eco-Efficient Products and Processes Laboratory (E2P2L), UMI 3464 CNRS-Solvay, 201108 Shanghai, People's Republic of China
[c] Laboratory for Chemical Technology (LCT), Department of Materials, Textiles and Chemical Engineering, Ghent University, Technologiepark 125, 9052 Ghent, Belgium
[d] Laboratoire de Physique de Solides, CNRS, Université Paris-Sud, Université Paris-Saclay, 91400 Orsay, France
[e] School of Physical Science and Technology, Shanghai Tech University, Shanghai 201210, People's Republic of China
[f] Institut Chevreul, FR2638 CNRS, Bât. C6 Université Lille 1, F-59655 Villeneuve d'Ascq, France
[g] IPCMS, UMR 7504 CNRS, Université de Strasbourg, 23 rue du Loess, BP 43, Cedex 2, 67034 Strasbourg, France
[h] Paul Scherrer Institute, CH-5232 Villigen, Switzerland

ARTICLE INFO

Keywords:
Solid micelles
Ru (III)
Hydrogenation
Biomass
Aqueous phase

ABSTRACT

Catalytic processes in water have a lower environmental impact, cost, and toxicity than in organic solvents. Considering the high content of water in biomass, it would be natural to use aqueous phase catalytic technology for the production of valuable products. However, in the aqueous phase, most metal-based catalysts suffer from low activity, low selectivity and deactivation due to metal oxidation and leaching. In this paper, we propose a solid micellar Ru catalyst (Ru(III)@MCM) based on single-site $Ru^{(III)}$ species stabilized by cetyltrimethylammonium (CTA^{+}) surfactant and immobilized in the walls of MCM-41 for the selective aqueous phase hydrogenation of carbonyl groups. This catalyst demonstrates exceptional selectivity, activity, and stability in comparison with conventional metallic catalysts. DFT modeling suggests that the reaction proceeds via heterolytic dissociation of hydrogen, forming a Ru-Hydride species, and subsequent hydride transfer to the carbonyl group. Water plays a key role in avoiding product inhibition.

1. Introduction

Biomass is the only available renewable carbon source with the potential to be used as a carbon-neutral feedstock [1]. Thus, the development of green and cost-efficient processes for transforming biomass-derived substrates into value-added chemicals is highly desirable [2]. To successfully achieve a sustainable future, efficient catalytic processes must be developed [3–5].

Approximately 70% of biomass is composed of water [6]. The most sustainable biomass pretreatment methods use water as a solvent [7–9]. For example, the hydrolysis of cellulose and hemicellulose over acid catalysts in an aqueous solution leads to glucose and xylose, with subsequent dehydration to hydroxymethylfurfural (HMF) and furfural, respectively [10–12]. From a Green Chemistry perspective [13], it is highly desirable to develop aqueous-based processes to transform biomass-derived molecules because it avoids changing solvents and the large energy costs associated with the removal of water [14].

Water is also an excellent solvent because it is cheap, abundant, and widely available [15]. It is non-flammable, non-toxic, and allows for easy separation of non-polar organic molecules by phase separation. Water also has a high heat capacity, enabling a more facile control of exothermic reactions, and its ability to form hydrogen bonds can influence substrates' reactivity [16]. In addition, water can induce transformations of biomass-based chemicals due to its mild acidity at high temperatures [17].

The hydrogenation of furan-based chemicals has been studied over supported heterogeneous transition metal catalysts such as Ni [18–20], Cu [9,21–24] and over supported noble metal such as Ru [4,11,25–29], Pd [30–33], and Pt [5,34]. Most heterogeneous catalysts hydrogenate the furan ring in addition to the carbonyl group, leading to a mixture of

E-mail addresses: UrbinaBlanco@UGent.be (C.A. Urbina-Blanco), Mark.Saeys@UGent.be (M. Saeys), Vitaly.Ordomsky@univ-lille.fr (V.V. Ordomsky).
[1] *equal contribution.*

https://doi.org/10.1016/j.apcatb.2021.120730
Received 13 July 2021; Received in revised form 11 September 2021; Accepted 13 September 2021
Available online 16 September 2021

furan and tetrahydrofuran-based alcohols [9,35,36].

Solvents can play a crucial role in tuning the selectivity towards specific furan-based species. Mironenko et al. observed hydrogenation of furfural to furfuryl alcohol with tetrahydrofurfuryl alcohol as a side product using water as a solvent over Pd and Ru nanoparticle catalysts supported on carbon, with lower activity of Ru nanoparticle catalysts due to the irreversible adsorption of water on the active sites [37]. Water was reported as an excellent solvent for the selective hydrogenation of furfural over Ru and Pt nanoparticles supported on reduced graphene oxide and on g-C_3N_4 [38]. Small size Ru nanoparticles incorporated into mesoporous zirconium silica, in Zr-MOF and in Al-MIL-53 demonstrated selective hydrogenation of furfural to furfuryl alcohol at mild reaction conditions [27,28,39]. The selectivity was assigned to a strong interaction between the Ru clusters and the support, creating active and selective $Ru^{\delta+}$ sites.

Water is often involved during catalytic reactions with the generation of new products. Thus, cyclopentanol and cyclopentenone were the main products during aqueous phase hydrogenation of furfural over Ni_xCo_y nanoparticles supported on carbon and over NiCu-50 nanoparticles supported on SBA-15, respectively, with no rearrangement products using alcohols as a solvent [11,40]. The opening of the ring was explained by the attack of a water molecule at the 5-position of furfuryl alcohol. Less polar solvents usually induce deeper hydrogenation than polar solvents. For example, Ni and Cu-nanoparticle-based catalysts supported on alumina and silica show high selectivity to methylfuran using hexane as a solvent [41]. The authors claim that the solvent plays a double role by stabilizing the product and modifying the intrinsic reactivity of the catalyst.

The application of aqueous phase hydrogenation reactions is often limited by several issues: catalysts based on reduced transition metals can be easily oxidized in the presence of water, leading to leaching of the metal during the reaction [40]; adsorption of water on noble metal nanoparticles lowers the activity [17,42] and homogeneous catalysts, especially those containing phosphine ligands, hydrolyze in the aqueous phase, losing their activity [42,43].

Single-site and single-atom catalysts (SSC and SACs) are an emerging family of materials that combine advantages of homogeneous and heterogeneous catalysts [40,44–46]: they display approximately 100% atomic utilization, relatively high stability, and easy separation from the reaction media [31]. For example, Pd SACs displayed superior activity for hydrogenation of succinic acid (SA) to g-butyrolactone [47]. Single Ru atoms supported over mesoporous graphitic carbon nitride facilitated either hydrogenation or HDO of lignin model compounds [48]. However, there are several drawbacks associated with the use/synthesis of these catalysts: most synthetic procedures require the use of expensive throw-away ligands and highly specialized equipment and techniques that hinder their scale-up production and applicability and the catalysts can be deactivated due to sintering and leaching of single atoms [31,46].

A solid micellar SSC **(Ru(III)@MCM)** was recently developed by the incorporation of $Ru^{(III)}$ atoms into the walls of MCM-41, stabilized by a cetyltrimethylammonium (CTA^+) surfactant [49]. Based on their structure, we explore the potential of these Ru(III)@MCM materials for the hydrogenation of polar carbonyl bonds in biomass-derived substrates. This solid micellar Ru catalyst shows high hydrogenation activity and carbonyl selectivity for biomass-derived chemicals in the aqueous phase. This type of catalyst resembles organometallic complexes and represents an easy and efficient way for heterogeneous use of oxidized Ru in catalysis.

Water plays a key role in the reaction with low activity in non-polar solvents. DFT modeling indicates that water stabilizes intermediates and transition states and, through competitive adsorption, prevents product inhibition.

2. Experimental section

2.1. Catalysts synthesis

The catalysts have been prepared using the standard procedure for MCM-41 synthesis [50] with the addition of $RuCl_3$ at the initial step (Fig. 1). In a typical synthesis, 1.3 mmol CTAB was added to 96 mL of deionized H_2O (Millipore system) together with 34 mL of ethanol under stirring. Afterward, $RuCl_3$ (J&K Scientific Ltd) was added to the mixture to provide a CTAB/$RuCl_3$ ratio of 3. This sample was denoted **Ru(III) @CTAB**.

The sample Ru(III)@MCM was prepared by mixing 10 mL of an aqueous ammonia solution with Ru(III)@CTAB under continuous stirring for 10 min. Then, 2 mL of TEOS (AR, Aladdin Chemical Regent Company) was poured into the solution with continuous stirring for 3 h at room temperature. The solid product was recovered by filtration, washed in water and dried overnight at room temperature. Besides this micellar catalyst, the two additional samples have been synthesized by adjusting the ratio of CTAB/Ru to 1 and 5. The sample prepared by subsequent ion exchange of CTA^+ by NH_4^+ has been denoted **Ru(III) @MCM-NH_4^+**.

Additionally, MCM has been prepared using the same procedure but without $RuCl_3$. The sample Ru/MCM was prepared by impregnation of MCM calcined at 450 °C (MCM-41) with $RuCl_3$ to obtain a Ru loading of 5 wt%, followed by calcination in air at 450 °C for 4 h and reduction at 200 °C for 2 h in fixed bed reactor. Ru/Al_2O_3 (5 wt% Ru loading) was purchased from Johnson Matthey Chemicals Company. Triphenylphosphine ruthenium chloride (TPRu) as a reference complex was purchased from Sigma Aldrich.

2.2. Characterization

For TEM analysis, a JEOL-2011F with an acceleration voltage of 200 kV was used. Before TEM characterization, the samples were dispersed in ethanol with ultrasonic treatment for 30 min and then dropped onto a carbon film on a copper grid. The water contact angle was measured by a contact angle tester (OCA20, Dataphysics). TGA was carried out on a SDT Q600 instrument between 25 and 800 °C under air/N_2. N_2 adsorption isotherms were collected by a volumetric gas adsorption analyzer (Quantachrome Instruments AutosorbiQ-MP-AG). XPS analysis has been performed by a ThermoFischer ESCALAB 250Xi photoelectron spectrometer using monochromated X-ray irradiation Al Kα (hv = 1486.7 eV) and 180° double-focusing hemispherical analyzer with a six-channel detector. The BE (binding energy) of the photoemission spectra was calibrated to the Si 2p peak with BE 103.4 eV for Si containing samples and to adventitious carbon C 1s peak with BE 284.8 eV. The Fourier transform infrared (FTIR) spectra were recorded using a Thermo Fisher Scientific Nicolet 6700 FTIR spectrometer (32 scans at a resolution of 4 cm^{-1}) equipped with a mercury cadmium telluride (MCT) detector. CO-FTIR experiments were performed in a vacuum cell (less than 10^{-5} torr). The catalyst samples for analysis were pressed in a 40–50 mg/cm^2 (D =13 mm) self-supporting discs. Before the analysis, all the samples were reduced at 90 °C for 3 h with subsequent vacuum treatment for 3 h. CO adsorption has been performed by the addition of CO doses in the cell at room temperature till full saturation. The H_2 temperature-programmed reduction (H_2-TPR) experiments were carried out by the AutoChem II 2920 apparatus. Quantitative elemental analyses were performed by inductively coupled plasma optic emission spectroscopy on a 720-ES ICP-OES (Agilent) with axially viewing and simultaneous CCD detection. The quantitative determination of metal content in the catalysts was based on the analysis of certificated standard solutions. The ICP ExpertTM software (version 2.0.4) provided metal concentrations in the samples. The detection limit is 0.1 ppm, and the accuracy is better than 5%.

XAS experiments at the Ru K edge (22,117 eV) were performed at the Super XAS beamline of the Swiss Light Source (PSI, Villigen,

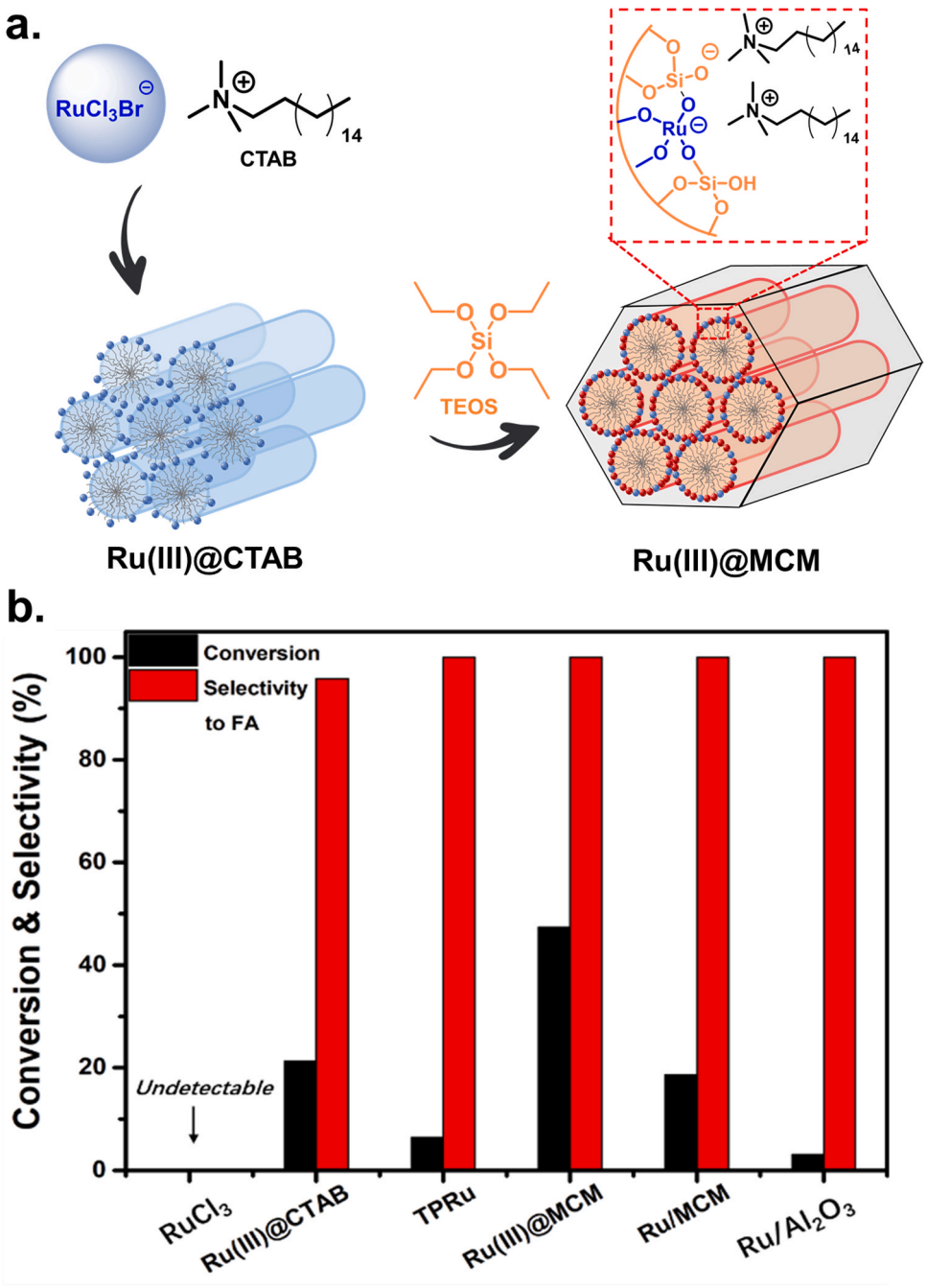

Fig. 1. Schematic structure of Ru(III)@MCM (a) and furfural hydrogenation performance for different Ru catalysts (b). Conditions: furfural/water: 0.3 g/4 g, 20 bar H_2, 70 °C, total Ru:12.8 μmol, 4 h.

Switzerland). The incident photon beam was selected by a Si(111) channel-cut monochromator from the polychromatic beam coming from 2.9 T superbend magnet. The EXAFS spectra were analyzed using the Demeter software package and fitted to the Fourier transformed, k^3-weighted signal for k = 3–14 $Å^{-1}$ with dk = 1 and for R = 1–4 Å with dR = 0.5. An amplitude reduction factor, S_0^2 = 0.81, was fitted using metallic Ru as a reference.

2.3. Catalysis

Hydrogenation reactions were conducted in a 40 mL stainless-steel autoclave reactor equipped with a magnetic stirrer, pressure gauge and an automatic temperature controller. In a typical experiment, 4 g of water, 0.3 g of reactant (furfural, levulinic acid, hydroxymethylfurfural, 2-acetylfuran, acetone or benzyl aldehyde) and 40 mg of catalyst or the same amount of Ru (12.8 μmol) were loaded into the reactor. The reactor was sealed, pressurized by 20 bar of H_2, and heated to the target temperature with continuous magnetic stirring. After the reaction, the autoclave was cooled down, the pressure was released, the solution was separated by filtration and the products were diluted by ethanol. The products were analyzed by GC (Agilent Technologies 7820 A, equipped with an HP-5 capillary column and flame ionization detector) with biphenyl as the internal standard. The products were identified by GC-MS (Agilent Technologies 5977 A MSD with Agilent Technologies 7890B GC system equipped with an HP-5 capillary column) and by ^1H NMR (Bruker Avance 400/300 NMR spectrometer).

The conversion of furfural, the selectivity and the yield to the product were defined as follows:

Conversion (%) = 1-n_A/n°_A;

Selectivity to the product p(%) =$n_p/(n^\circ_A-n_A)$;

Yield (%) = Conversion × Selectivity,

where n_A and n°_A refer to the final and the initial number of moles of furfural, respectively. n_p is the number of moles of converted furfural to the product p.

2.4. Computational methods

Density functional theory (DFT) calculations were performed using Gaussian16.[51] The active site was modeled using a cluster model of 17 Si, 32O, 12H and 1 Ru atoms. During geometry optimizations, the bottom part of the cluster (6 Si, 8O and 6H atoms) was kept fixed. The PBE0 functional was used in combination with the Grimme's D3 dispersion correction and the Becke-Johnson damping function (D3(BJ)) [52,53]. Gibbs free energies were obtained by combining electronic energies with standard thermal and entropy corrections from the vibrational frequencies. Ahlrich's Def2-SVP basis set was used for geometry optimizations and frequency calculations, while electronic energies were obtained with the larger Def2-TZVP basis set [54]. The chemical potential for water was obtained from a cluster of four molecules of H_2O. These small structures $(H_2O)_n$ with n = 3–5, are stable and sufficient to account for the desorbed water not interacting with the catalyst surface [55].

3. Results and discussion

3.1. Furfural hydrogenation activity of Ru(III)@MCM

The hydrogenation of furfural to furfuryl alcohol (FA) was selected as a model reaction to compare the activity of solid micellar Ru(III)@MCM with homogeneous ($RuCl_3$, TPRu) and heterogeneous supported (Ru/MCM, Ru/Al_2O_3) Ru-based catalysts in the aqueous phase (Fig. 1). The reaction was performed at mild conditions of 70 °C and 20 bar of H_2. Two main products were detected: furfuryl alcohol (FA) and tetrahydrofurfuryl alcohol (THFA). $RuCl_3$ dissolved in water also exhibited no activity for furfural hydrogenation. The addition of cetyltrimethylammonium bromide (CTAB) in the presence of ethanol to the aqueous $RuCl_3$ solution (Ru@CTAB) increases the furfural conversion to 21.3% with a furfuryl alcohol selectivity of 95%.

In ethanol aqueous solutions, long chain quaternary ammonium surfactants such as CTAB form cylindrical micelles (Fig. 1a). In the presence of $RuCl_3$, the micelles form an adduct with the generation of $[CTA]^+[Br]^-$ and $[CTA]^+[Ru^{(III)}BrCl_3]^-$ ion pairs. Hydrolysis of the micelles with TEOS leads to the growth of the silica walls around the agglomerated micelles, with the incorporation of $Ru^{(III)}$ in the silica walls of MCM-41 (Fig. 1a) [49]. It should be noted that, contrary to other mesoporous-based materials, we preserve the CTA^+ surfactant in the pores of the Ru(III)@MCM catalyst. Since the Ru/CTAB ratio in the micelles is about 3, the $[CTA]^+[Br]^-$ are converted to basic $[CTA]^+[SiO]^-$ ion pairs (Fig. 1a). Heterogenization of the micelles to form Ru(III)@MCM further increases the hydrogenation activity per Ru and

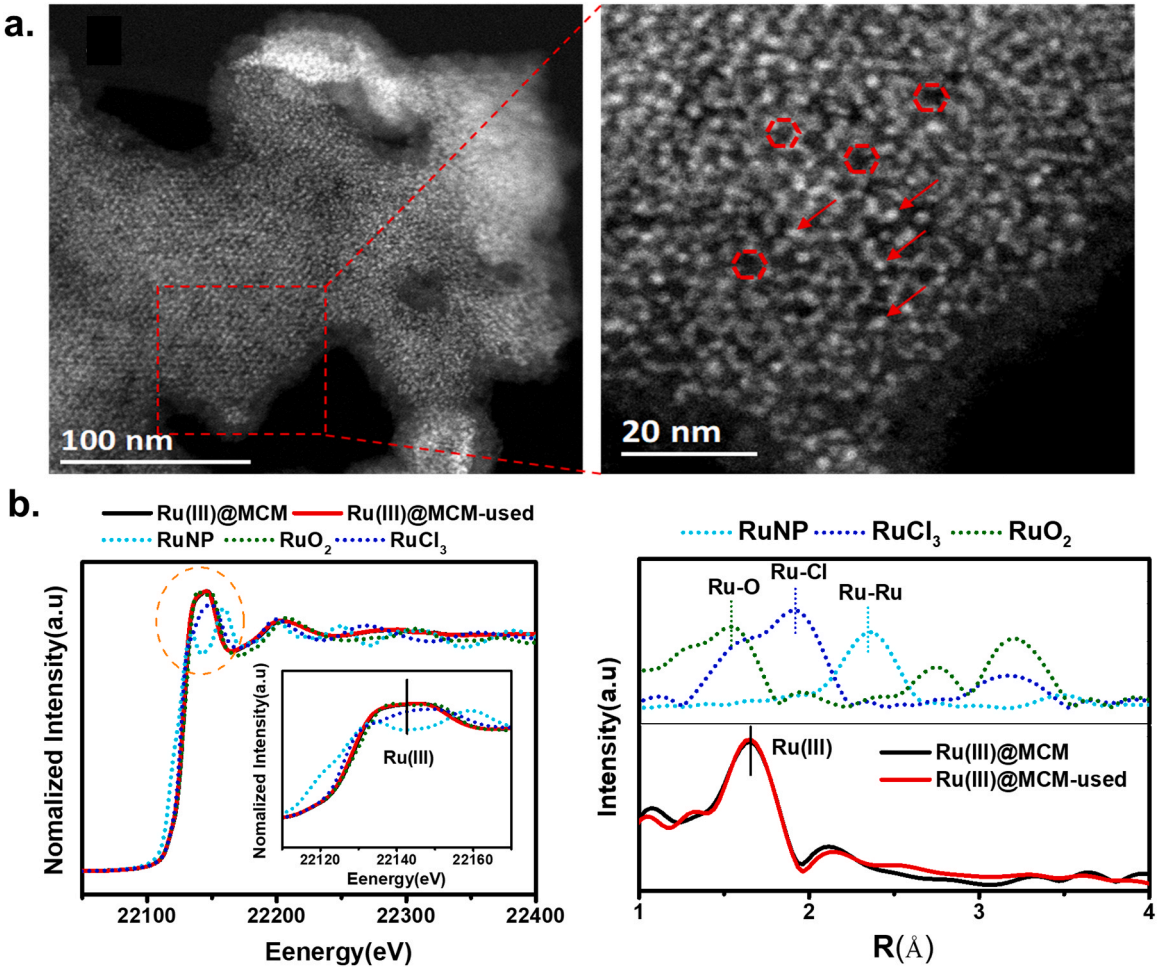

Fig. 2. STEM-HAADF image of Ru(III)@MCM sample (a) and Ru K-edge XANES spectra and Fourier transformed χ(k)-functions of the EXAFS spectra of Ru catalysts (b).

improves the separability of the catalyst. Ion exchange of the CTA^+ surfactant with NH_4^+ significantly decreases the activity of Ru(III)@MCM, establishing that the CTA^+ surfactant plays an important role in the catalytic activity.

The prepared Ru(III)@MCM material contains 3.2 wt% of Ru (Table S1, SI) and CTA contributes about 45 wt% of the mass of Ru(III)@MCM catalyst (Fig. S1, SI and Fig. S2a, SI). Identification of the individual $Ru^{(III)}$ atoms was confirmed using STEM-HAADF. The sensitivity of this method depends on the Z atomic number, and highlights Ru atoms (44) over Si atoms (14). The uniform distribution of individual Ru atoms in the walls of Ru(III)@MCM (Fig. 2a, Fig. S3, SI) was observed before and after ion exchange of CTA^+ with NH_4^+. In contrast, the Ru/MCM catalyst prepared by impregnation shows the presence of small Ru nanoparticles (Fig. S4, SI).

The electronic state of $Ru^{(III)}$ was studied by XPS and XAS. The Ru(III)@MCM XANES spectrum (Fig. 2b) is similar to that of RuO_2 and $RuCl_3$ indicating the oxidized state of Ru in the catalyst. The Fourier transform (FT) EXAFS moduli of the Ru(III)@MCM sample (Fig. 2b) (without phase shift) show a spectrum similar to that of RuO_2 with slightly longer Ru-O distances. Fitting the Ru(III)@MCM EXAFS indicates that the Ru atoms are coordinated by 3.3 ± 0.5 oxygen neighbors located at 2.07 ± 0.01 Å (Fig. S5, SI). Peaks corresponding to metallic Ru—Ru and contiguous Ru-O-Ru bonds, expected to be around 2.4 and 3.3 Å, were not detected. Ru—Cl bonds, detectable in the EXAFS of $RuCl_3$ at around 2.0 Å, were also not detected in Ru(III)@MCM. The weak peak observed at 2.2 Å may be related to an additional longer Ru-O bond, however, the quality of the EXAFS data was not sufficient to reliably assign this feature.

The XAS analysis has been supported by XPS results (Fig. S6, SI). The Ru/MCM spectrum is characterized by a Ru 3p3/2 peak at 460.6 eV indicating the presence of metallic Ru with the contribution of the peak of oxidized Ru at 463.5 eV most probably localized on the surface of Ru nanoparticles [56]. In the Ru(III)@MCM catalyst, the Ru 3p3/2 peak is shifted to 462.3 eV due to the change of the oxidation state to $Ru^{(III)}$. Additionally, the peak at 465.3 eV is observed, which could be assigned to the presence of Ru oxide species similar to those in Ru/MCM and non-coordinated by CTA^+. H_2-TPR shows (Fig. S7, SI) the peak at the temperature about 100 °C with an additional broad peak at about 200 °C over Ru(III)@MCM, which could be attributed to reduction combined with the decomposition of surfactant at higher temperatures. It is different in comparison with a single reduction peak of RuO_2 in Ru/MCM at 175 °C. CO-FTIR analysis of Ru/MCM demonstrates the presence of the peak at 1983 cm^{-1}, which according to the literature corresponds to the linearly bonded CO on zerovalent Ru sites (Fig. S8, SI) [57]. Ru(III)@MCM contains peaks at higher wavenumbers 2006 and 2076 cm^{-1}, which could be assigned to carbonyl species on oxidized Ru sites, (i.e., $Ru^{n+}(CO)_x$) [57].

Thus, characterization of the Ru(III)@MCM material indicates the incorporation of Ru single sites in the walls of MCM-41. The high stability of CTA^+ in the material indicates ionic interaction between CTA^+ and $Ru(OSi)_4^-$ species in the pores (Fig. 1a).

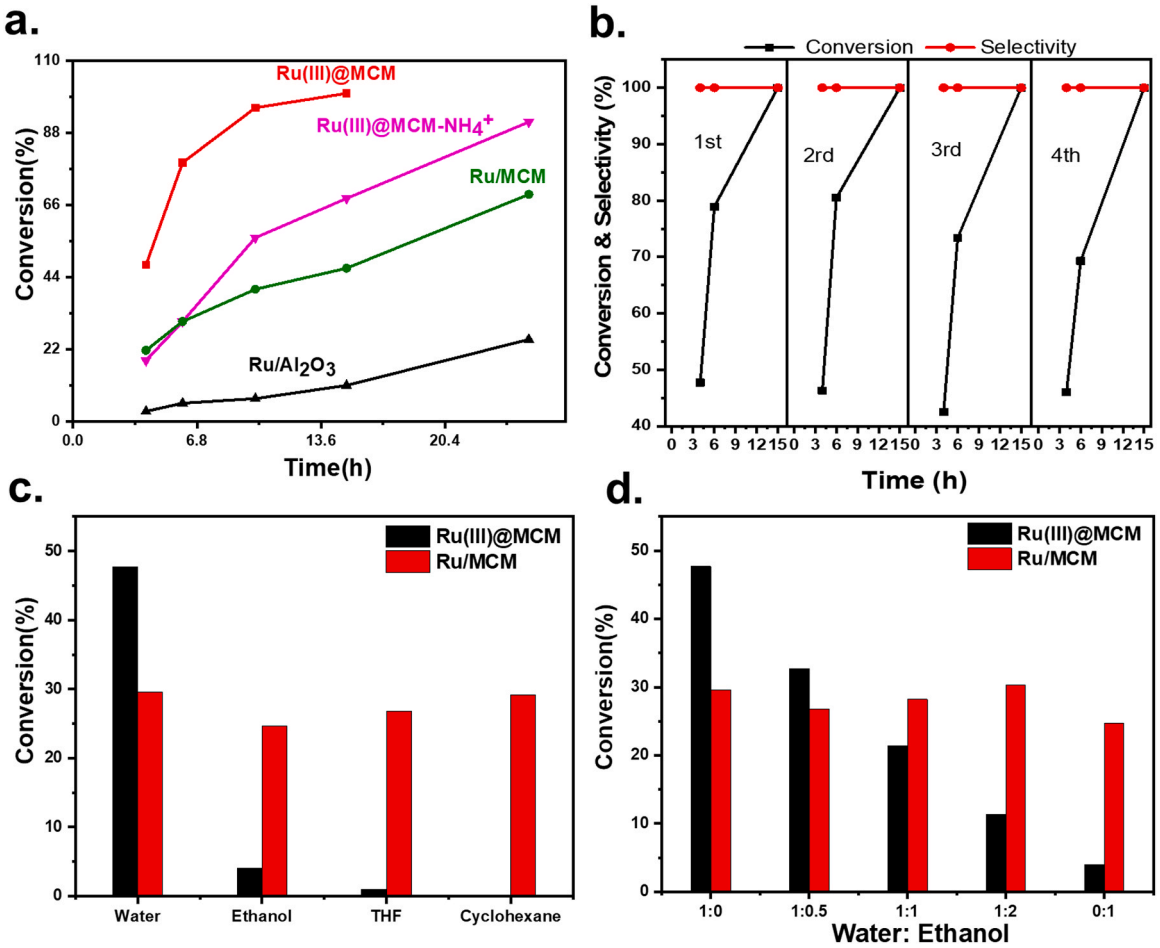

Fig. 3. Aqueous phase furfural hydrogenation activity of Ru(III)@MCM and of reference supported Ru catalysts (a); performance stability of Ru(III)@MCM for 4 cycles (b); effect of the solvent on the furfural conversion over Ru(III)@MCM and supported Ru/MCM (c); effect of the water/ethanol ratio on the furfural conversion over Ru(III)@MCM and supported Ru/MCM (d). Conditions: furfural/water (or organic solvent): 0.3 g/4 g, 20 bar H_2, 70 °C, total Ru:12.8 μmol, 4 h.

3.2. Recyclability and solvent effects on the activity of Ru(III)@MCM

The activity of Ru(III)@MCM was compared with supported heterogeneous Ru catalysts for the aqueous phase hydrogenation of furfural (Fig. 3). Ru(III)@MCM is much more active than the reference materials, reaching full conversion after 10 h (Fig. 3a). Decreasing the CTA/Ru ratio from 5 to 1 in the solid micellar catalysts significantly decreases the catalytic activity (Fig. S9, SI), most likely due to the reduced stability of the $Ru^{(III)}$ sites and their agglomeration forming Ru nanoclusters for low CTA to Ru ratios.

To investigate the stability and reusability of Ru(III)@MCM, the catalyst was separated by centrifugation, washed with water/ethanol, and tested in the next furfural hydrogenation cycle. As seen in Fig. 3(b), Ru(III)@MCM continues to achieve full conversion after 4 recycling cycles with no changes in selectivity, yet, a small decrease in the conversion after 6 h can be observed.

Characterization of the catalyst after reaction by TG and ICP with ^1H NMR analysis of the solvent (Fig. S2, SI) shows a small loss of CTA (about 5 wt%) after the first reaction cycle with no changes in the composition of the catalyst after the next cycles (Table S1, SI). The high stability of CTA^+ in the material suggests that there is an ionic interaction between CTA^+ and $Ru(OSi)_4^-$ species. Analysis of the electronic state of Ru by XAS and XPS in the used catalyst (Fig. 2 and Fig. S6, SI) demonstrates that the oxidation state of $Ru^{(III)}$ does not change after reaction. STEM-HAADF analysis (Fig. S3, SI) shows that Ru(III)@MCM has the same single site Ru species after reaction. Substitution of CTA^+ by NH_4^+ results in the formation of Ru nanoclusters after reaction, demonstrating the important role of CTA^+ in stabilizing the single site $Ru^{(III)}$ species in the walls of MCM-41 (Fig. S3, SI).

The solvent plays a key role in the hydrogenation of furfural over heterogeneous catalysts. Traditionally, organic solvents are used for the hydrogenation of furfural [31,45] due to the low solubility of furfural in water and the detrimental effect of water on metallic catalysts. Earlier publications claim positive effects of nanosheet carbon supports on the aqueous phase catalytic performance due to the higher dispersibility of the catalyst in water [38]. The formation of hydrogen bonds between water and biomass-based substrates or transition states can also affect their reactivity as observed for Diels-Alder reactions in polar solvents [14,58].

To evaluate the solvent effect for Ru(III)@MCM, furfural hydrogenation was tested in cyclohexane, tetrahydrofuran (THF), ethanol, and water (Fig. 3**c**). Water has a dramatic effect on the activity of Ru(III)@MCM. The highest activity was observed in water and the activity decreases significantly with the polarity of the solvent. No activity was observed in non-polar cyclohexane. Increasing the ethanol/water ratio in ethanol/water mixtures also decreases the activity of Ru(III)@MCM (Fig. 2d). Analysis of the kinetics of furfural hydrogenation over Ru(III)@MCM in different solvents demonstrates high initial activity in organic solvents followed by deactivation (Fig. S10, SI). The mass transfer limitation would slow down reaction without deactivation of the catalyst [59]. The solvent has a limited effect on the activity of supported Ru/MCM, although the activity slightly increases when water is replaced by less polar solvents.

To further quantify the effect of water on the activity, we compared furfural hydrogenation in pure furfural and furfural/water (Fig. S11, SI). Again, water significantly enhances the activity, increasing the yield by approximately 45%.

To analyze the effect of the CTA^+ surfactant on the hydrophobicity of the Ru(III)@MCM material, we used contact angle measurements (Fig. 4). The contact angle of 64° for a water droplet on Ru(III)@MCM is much higher than for Ru/MCM (25°), pointing to a significantly higher hydrophobicity of the material [60]. The hydrophobicity of Ru(III)@MCM leads to a different partitioning of the catalyst material in the biphasic reaction mixture containing furfural and water (Fig. 4). While Ru/MCM is found mainly at the bottom of the vial and dissolved in the aqueous phase, Ru(III)@MCM has a strong amphiphilic character and

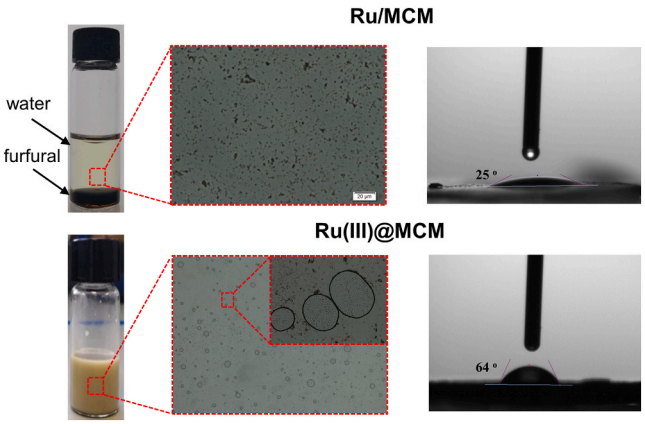

Fig. 4. The microscopy images of Ru(III)@MCM and Ru/MCM in the water/furfural biphasic system with contact angle between water droplet and catalysts.

even stabilizes the furfural/water emulsion. Ru(III)@MCM particles can be found at the interface between water and furfural, resembling a pickering emulsion system [61]. The catalytic reaction in water can reinforce the hydrophobic interaction of furfural with CTA in the pores of Ru(III)@MCM leading to a high local concentration of furfural in the pores of the catalyst.

To evaluate the possible direct participation of water in the reaction route, we tested the hydrogenation of furfural in isotope-labeled H_2O^{18}. The presence of water leads to the formation of small amounts of geminal diol species from aldehyde in an aqueous solution [62,63], possibly opening up an alternative hydrogenation route. On the other hand, the formation of a gem-diol moves the aldehyde away for the more reduced alcohol product.

Fig. 5 shows the furfural and furfuryl alcohol mass spectra after furfural hydrogenation in H_2O^{18} for low furfural conversions. Hydrogenation of furfural over Ru(III)@MCM in H_2O^{18} results in the formation of a mixture of alcohols with *m/z* of 100 and 98, in addition to unconverted furfural with *m/z* of 98 and 96, showing the rapid incorporation of O^{18} both in furfural and furfuryl alcohol. In contrast, almost no O^{18} incorporation is observed over Ru/MCM. Over Ru-free, surfactant-containing MCM, O^{18} is also rapidly incorporated in furfural, suggesting that the gem-diol mediated O^{18} exchange is catalyzed by the SiO^- basic

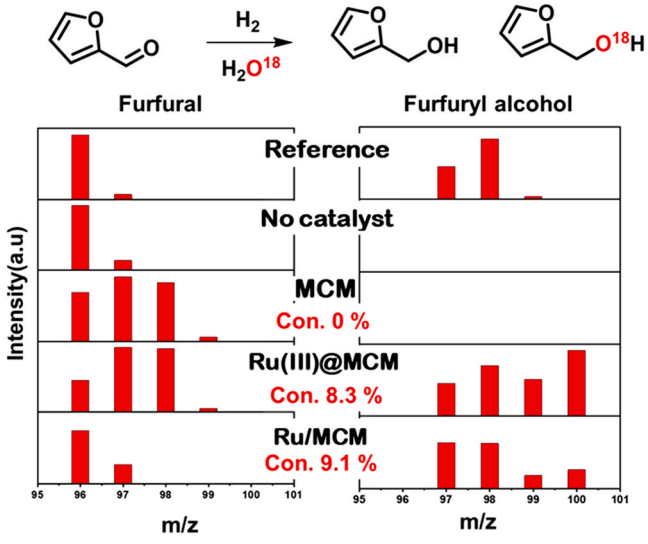

Fig. 5. GC-MS mass spectrum of furfural and furfural alcohol during hydrogenation of furfural in labeled H_2O^{18}. Conditions: 20 bar H_2, 40 °C, 10 mg catalyst, 1–3 h; Furfural/ H_2O^{18} mass ratio:1/10. Furfural conversions < 10%.

sites in surfactant-containing MCM-41 (Fig. 1a).

The effect of the catalyst and the solvent on the selectivity between C═C and C═O hydrogenation was investigated for cinnamaldehyde (Fig. 6). Conventional Ru/MCM and Ru/Al_2O_3 are more selective (58–62% of hydrocinnamaldehyde, HCAL) for the thermodynamically more favorable C═C hydrogenation (ΔH = −134 kJ/mol) than for C═O hydrogenation (ΔH = −66 kJ/mol) due to direct hydrogenation of the non-polar C═C double bond by dissociated hydrogen on the metallic Ru surface [9]. However, aqueous phase hydrogenation over Ru(III)@MCM is rather selective for the polar C═O double bond, with a cinnamyl alcohol (COL) selectivity of 69%. When the water solvent is replaced by ethanol and cyclohexane, the selectivity for C═O hydrogenation decreases but remains superior to conventional metallic Ru nanoparticle catalysts. Analysis of the catalytic performance at different reaction times demonstrates no significant effect of the conversion on the selectivity (Fig. S12, SI). The preferential hydrogenation of C═O of cinnamaldehyde could be assigned to heterolytic dissociation of hydrogen over single site $Ru^{(III)}$ species as compared with homolytic dissociation of hydrogen over a metallic Ru surface. The interaction of carbonyl group with charged $Ru^{(III)}$ could also play the role in the tuning of the selectivity during the hydrogenation of cinnamaldehyde to COL by preferential interaction with carbonyl group similar to the effect observed during the addition of electropositive metals such as Ga, In or Sn to Co or Ru [64,65].

3.3. Substrate scope

The hydrogenation of other biomass-derived and model molecules containing carbonyl groups such as levulinic acid, hydroxymethylfurfural (HMF), 2-acetylfuran, levulinic acid, acetone, benzyl aldehyde, 1-butanal, 1-octanal etc. was explored to evaluate the substrate scope of Ru(III)@MCM (Fig. S13, SI). Fig. 7 and Fig. S14-S17, SI demonstrates that Ru(III)@MCM is highly active and selective for the

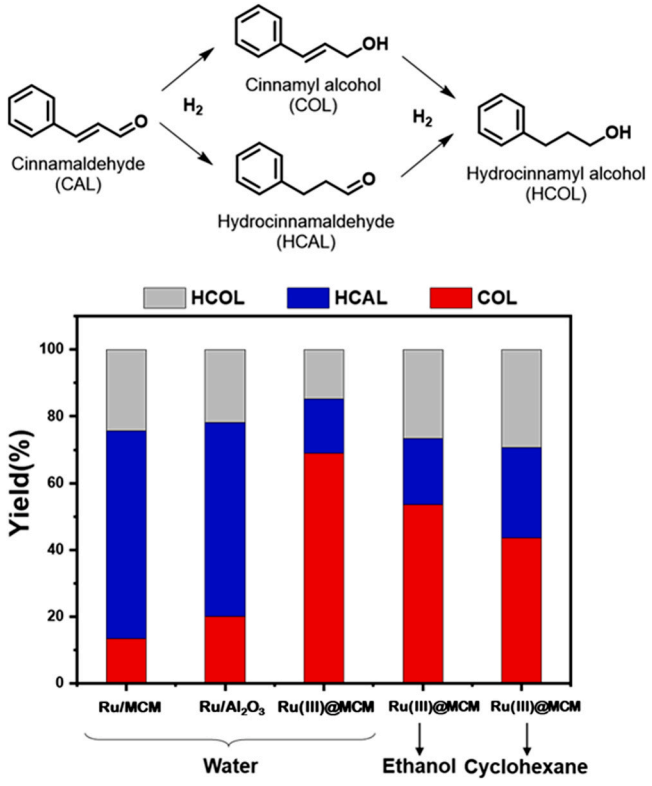

Fig. 6. Effect of catalyst and solvent on the selectivity between C═O and C═C hydrogenation for cinnamaldehyde. Conditions: 20 bar H_2, 40 °C, 40 mg catalyst, 2–15 h; cinnamaldehyde/solvent:0.1 g/4 g, conversion 100%.

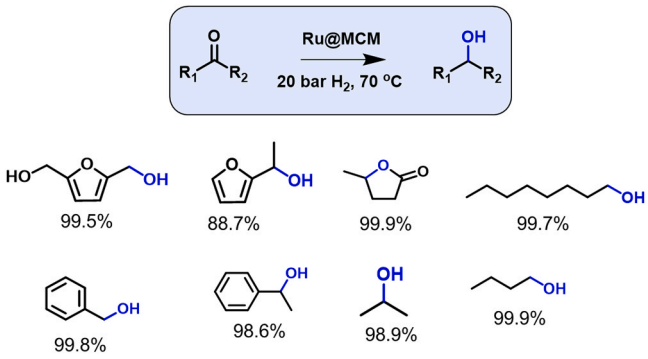

Fig. 7. Scope of Ru(III)@MCM for the hydrogenation of the carbonyl group in biomass-derived and model substrate molecules (yield) (20 bar H_2, 70 °C, 40 mg catalyst, 15 h; substrate/H_2O: 0.3 g/4 g).

hydrogenation of these carbonyl groups, and this under aqueous conditions and at a temperature that is milder (70 °C) than for conventional supported metallic catalysts (Table S2, SI). The catalytic activity of Ru(III)@MCM is superior to the reference-supported Ru catalysts (Fig. S13, SI).

3.4. Molecular modelling

Density functional theory (DFT) calculations were performed to analyze the reaction mechanism of the selective hydrogenation of aldehydes catalyzed by Ru(III)@MCM in an aqueous environment. The cluster model used to describe the active site is based on silsesquioxane cages, as reported by Feher [66] and Liu [45] (Fig. 8). Since structural and electronic effects of the active Ru site are dominated by the local structure, cluster calculations sufficiently reproduce the reactivity of the metal center and the silica ring strain for single-atoms catalysts in MCM-41 [45,66]. The model consists of a $Ru^{(III)}$ single-site coordinated to the silica framework by 4 oxygens [49]. The cluster contains 17 Si atoms and 2 silanol groups. The cluster is terminated with hydrogen atoms. Termination instead with OH groups did not influence the reactivity at the Ru site. The surfactant (CTA^+) was not included in the model, but the overall cluster was negatively charged to account for the positive charge on the surfactant, establishing the $[Ru^{(III)}@17\text{-}Si]^-[CTA]^+$ ion-pair. Analysis of the electron density shows that the negative charge is shared between Ru and its adjacent oxygens [49].

Water enhances the activity of Ru(III)@MCM and the solvent hence interacts with the walls of MCM-41. In this work, we use water in a liquid state as a reference (see *Computational Methods*), however, the actual chemical potential of water inside the surfactant-filled pores of MCM-41 is not well-known. To obtain a realistic resting state for the active site, we considered the adsorption of water, ethanol, furfural, and furfuryl alcohol at the $Ru^{(III)}$ site (Fig. S18, SI). The calculations show that $Ru^{(III)}$ prefers a hexacoordinated structure with 2 ligands and that ethanol adsorbs stronger than water. This strong adsorption of ethanol could hinder the reaction since at least one ligand needs to desorb to allow reaction. The fast deactivation of the micellar catalyst in ethanol after initial hydrogenation activity supports this assumption (Fig. S10, SI). Thus, changing of the polarity of the solvent affects the coordination ability and activity of the catalyst. The strong effect of solvents on the catalytic performance of homogeneous catalysts is usually assigned to coordination with the metal sites or interactions with the ligands [67]. For example, the isomerization of allylic alcohol to propanal over Fe$(CO)_4$ depends strongly on the solvent basicity with full inhibition of the catalytic activity using basic solvents suppressing alkene adsorption [68]. The effect of solvent on the catalytic performance of conventional heterogeneous metallic catalysts is less pronounced, which is fully consistent with our catalytic results.

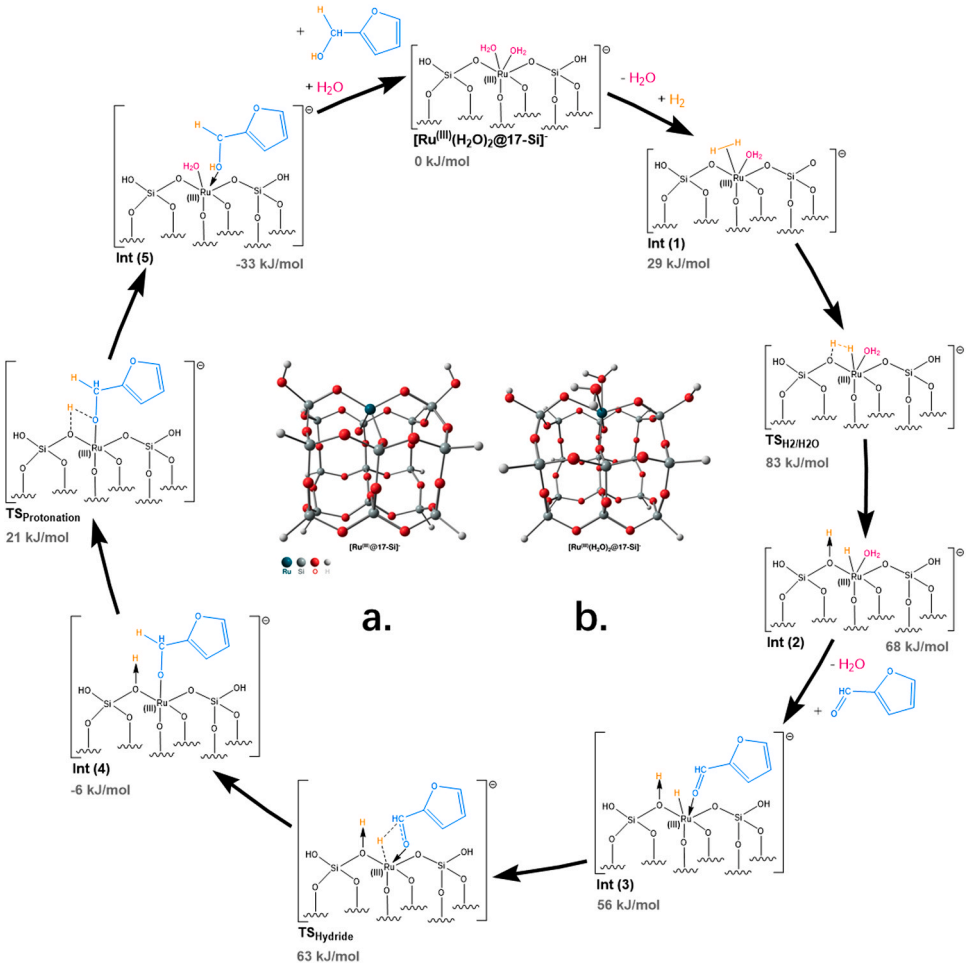

Fig. 8. Cluster models of $[Ru^{(III)}@17\text{-}Si]^-$ for (a), $[Ru^{(III)}(H_2O)_2@17\text{-}Si]^-$ for (b), and catalytic cycle for the hydrogenation of furfural following the alkoxide path over a $[Ru^{(III)}(H_2O)_2@17\text{-}Si]^-$ cluster. DFT calculations were performed with PBE0-D3(BJ)/def2-TZVP//PBE0-D3(BJ)/def2-SVP at 298 K and 1 atm.

The model with 2 adsorbed water molecules, designated as $[Ru^{(III)}(H_2O)_2@17\text{-}Si]^-$, is shown in Fig. 8 and was used as the starting structure to analyze the reaction path. The bare catalyst is represented by $[Ru^{(III)}@\ 17\text{-}Si]^-$.

The most favorable cycle and Gibbs free energy profile for the hydrogenation of furfural is shown in Fig. 8 and Fig. S19, SI, respectively. Starting from the water-saturated $Ru^{(III)}$ site, the most favorable pathway starts with the adsorption and heterolytic dissociation of H_2. For this step, one water molecule needs to desorb from the active site. The associated free energy barrier, 83 kJ/mol, is the highest along this reaction pathway. Next, the second reactant, furfural, displaces the second water molecule. Interestingly, this step is slightly exergonic, showing that the relative adsorption energy of water and furfural depends on the state of the $Ru^{(III)}$ active site. There are two plausible routes for the formation of the alcohol: one involving the formation of an alkoxide intermediate and another via a hydroxyalkyl intermediate. In the alkoxide path, hydride transfer to the carbonyl group of furfural is followed by the protonation of the alkoxide.

In the hydroxyalkyl pathway, protonation of the carbonyl group is the first step. The barrier to form the alkoxide is 21 kJ/mol higher than the barrier to form the hydroxyalkyl species (Fig. S20, SI). This can be related to the basicity of the catalyst. The proton has a higher affinity for the OSi than for the C═O bond, indicating that the oxygens around Ru are more basic than the O of the carbonyl. It could be noted that these protons may move to even more basic sites in the MCM-41 structure. However, to simplify the DFT calculations, the H^+ was kept at the OSi next to Ru. Hydride transfer to the carbonyl group is relatively facile and very favorable. Several pathways were considered for the protonation of the alkoxy species. As $Ru^{(III)}$ is formally penta-coordinated in Int(4), additional water could adsorb at the Ru site. Alternatively, a water molecule could act as a shuttle for the proton transfer from the Si-OH group to the alkoxy species, which has been observed earlier [69]. In this manner, water is involved in the reaction without direct coordination with the catalyst. The most favorable pathway is shown in Fig. 8 and is calculated to be the direct transfer of the SiOH proton to the alkoxy species. The displacement of furfural alcohol by a water molecule closes the catalytic cycle. In Fig. S21, SI, the energy profile is shown for the bare $[Ru^{(III)}@\ 17\text{-}Si]^-$ cluster, neglecting the adsorption of water. Comparing the energy span of both profiles shows that considering the adsorption of water leads to a faster reaction. The effect of the solvent was also considered by comparing the energy profile with ethanol and with water (Fig. S22-S24, SI). The stronger adsorption of ethanol increases the energy span for the reaction, likely reducing the catalytic activity.

The calculations show that the hydrogenation of carbonyl groups over $Ru^{(III)}$ single site solid micellar catalyst proceed by heterolytic dissociation of hydrogen (Fig. S24, SI) and the increased performance of the catalyst in the presence of water lies in the competitive adsorption between reactants, products, and solvent molecules, assisting in preventing product inhibition. Adsorption of the solvent molecules on $Ru^{(III)}$ displaces the product from the active site. This strategy is different from homolytic hydrogen activation over conventionally used metallic catalysts (Table S2, SI). It can be observed that conventional catalysts require higher reaction temperature and usually organic solvents. At the

same time the selectivity is often relatively low due to non selective hydrogenation of different types of functional groups. The advantage of single site micellar catalyst is that heterolytic dissociation of hydrogen provides an opportunity to eliminate hydrogenation of non polar groups such as aromatic rings or double bond of olefin. At the same time, the non metallic character of the active sites in solid micellar catalyst makes it non sensitive to poisoning agents, which is important for the conversion of biomass based molecules.

4. Conclusions

A solid micellar Ru(III)@MCM catalyst with single-site $Ru^{(III)}$ incorporated in the walls of MCM-41 and quaternary ammonium surfactant in the pores efficiently catalyzes the selective hydrogenation of carbonyl group in biomass-derived molecules in the aqueous phase at mild conditions. The catalyst provides significantly higher activity and selectivity in comparison with conventional metallic catalysts.

DFT suggests that the hydrogenation of furfural to furfuryl alcohol proceeds via heterolytic dissociation of H_2, which is rate-limiting. The subsequent steps involve hydride transfer to the carbonyl group, followed by protonation. Calculations also show that one of the possibilities to describe the increased performance of the catalyst in the presence of water lies in the competitive adsorption between reactants, products and solvent molecules, assisting in preventing product inhibition. Adsorption of the solvent molecules on $Ru^{(III)}$ displaces the product from the active site. However, the strength of this adsorption must be carefully balanced since strong adsorption inhibits the activity.

CRediT authorship contribution statement

Qiyan Wang: Investigation, Writing – original draft. **Sara Santos:** Methodology, Writing – original draft. **César A. Urbina-Blanco:** Methodology, Writing – review & editing. **Wenjuan Zhou:** Methodology. **Thuriot Joelle:** Investigation. **Yong Yang:** Investigation. **Svetlana Heyte:** Investigation. **Maya Marinova:** Investigation, Data curation. **Ovidiu Ersen:** Data curation. **Walid Baaziz:** Investigation. **Olga Safonova:** Investigation. Data curation, Writing – original draft. **Mark Saeys:** Supervision, Writing – review & editing, Funding acquisition. **Vitaly V. Ordomsky:** Supervision, Writing – review & editing, Funding acquisition, Project administration.

Declaration of Competing Interest

The authors declare that they have no known competing financial interests or personal relationships that could have appeared to influence the work reported in this paper.

Acknowledgements

The authors acknowledge the financial support of the French National Research Agency (NANO4-FUT, Ref. ANR-16-CE06-0013) and Solvay. Chevreul Institute and the TEM facility in Lille is supported by the « Ministère de l'Enseignement Supérieur et de la Recherche », the Conseil Regional du Nord-Pas de Calais and the European Regional Development Fund (ERDF). Sara Santos, César A. Urbina-Blanco and Mark Saeys acknowledge the support from VLAIO with the cluster SBO project CO2PERATE (project number HBC.2017.0692) and from UGent High-Performance Computing (HPC). The computational resources (Stevin Supercomputer Infrastructure) and services used in this work were provided by the VSC (Flemish Supercomputer Center), funded by Ghent University, FWO and the Flemish Government – department EWI. César A. Urbina-Blanco acknowledges financial support from a senior postdoctoral fellowship from the Fund for Scientific Research Flanders (FWO). We thank the Swiss Light Source for providing beamtime at the SuperXAS beamline.

Appendix A. Supporting information

Supplementary data associated with this article can be found in the online version at doi:10.1016/j.apcatb.2021.120730.

References

[1] B. Boekaerts, B.F. Sels, Catalytic advancements in carboxylic acid ketonization and its perspectives on biomass valorisation, Appl. Catal. B: Environ. (2020), 119607.
[2] P. Gallezot, Conversion of biomass to selected chemical products, Chem. Soc. Rev. 41 (2012) 1538–1558.
[3] M. Besson, P. Gallezot, C. Pinel, Conversion of biomass into chemicals over metal catalysts, Chem. Rev. 114 (2014) 1827–1870.
[4] R. Insyani, A.F. Barus, R. Gunawan, J. Park, G.T. Jaya, H.S. Cahyadi, M.G. Sibi, S. K. Kwak, D. Verma, J. Kim, RuO2–Ru/Hβ zeolite catalyst for high-yield direct conversion of xylose to tetrahydrofurfuryl alcohol, Appl. Catal. B: Environ. 291 (2021), 120120.
[5] Y. Li, J. Ma, D. Jin, G. Jiao, X. Yang, K. Liu, J. Zhou, R. Sun, Copper oxide functionalized chitosan hybrid hydrogels for highly efficient photocatalytic-reforming of biomass-based monosaccharides to lactic acid, Appl. Catal. B: Environ. 291 (2021), 120123.
[6] C. Barrett, J. Chheda, G. Huber, J. Dumesic, Single-reactor process for sequential aldol-condensation and hydrogenation of biomass-derived compounds in water, Appl. Catal. B: Environ. 66 (2006) 111–118.
[7] Q.-V. Bach, O. Skreiberg, Upgrading biomass fuels via wet torrefaction: a review and comparison with dry torrefaction, Renew. Sustain. Energy Rev. 54 (2016) 665–677.
[8] L. Yan, R. Ma, L. Li, J. Fu, Hot water pretreatment of lignocellulosic biomass: an effective and environmentally friendly approach to enhance biofuel production, Chem. Eng. Technol. 39 (2016) 1759–1770.
[9] Y.-A. Chen, H. Yang, D. Ouyang, T. Liu, D. Liu, X. Zhao, Construction of electron transfer chains with methylene blue and ferric ions for direct conversion of lignocellulosic biomass to electricity in a wide pH range, Appl. Catal. B: Environ. 265 (2020), 118578.
[10] J. Esteban, A.J. Vorholt, W. Leitner, An overview of the biphasic dehydration of sugars to 5-hydroxymethylfurfural and furfural: a rational selection of solvents using COSMO-RS and selection guides, Green Chem. 22 (2020) 2097–2128.
[11] X. Gao, S. Zhu, M. Dong, J. Wang, W. Fan, Ru/CeO_2 catalyst with optimized CeO_2 morphology and surface facet for efficient hydrogenation of ethyl levulinate to γ-valerolactone, J. Catal. 389 (2020) 60–70.
[12] J.-Y. Yeh, B.M. Matsagar, S.S. Chen, H.-L. Sung, D.C. Tsang, Y.-P. Li, K.C.-W. Wu, Synergistic effects of Pt-embedded, MIL-53-derived catalysts (Pt@ Al_2O_3) and $NaBH_4$ for water-mediated hydrogenolysis of biomass-derived furfural to 1, 5-pentanediol at near-ambient temperature, J. Catal. 390 (2020) 46–56.
[13] P. Anastas, J. Warner, Green Chemistry: Theory and Practice, Oxford Univ Press, 1998.
[14] A. Kruse, N. Dahmen, Water – a magic solvent for biomass conversion, J. Supercrit. Fluids 96 (2015) 36–45.
[15] G. Singh, L. Singh, J. Gahtori, R.K. Gupta, C. Samanta, R. Bal, A. Bordoloi, Catalytic hydrogenation of furfural to furfuryl alcohol over chromium-free catalyst: enhanced selectivity in the presence of solvent, Mol. Catal. 500 (2021), 111339.
[16] R.M. Mironenko, O.B. Belskaya, V.P. Talsi, V.A. Likholobov, Mechanism of Pd/C-catalyzed hydrogenation of furfural under hydrothermal conditions, J. Catal. 389 (2020) 721–734.
[17] M.A. Mellmer, C. Sener, J.M. Gallo, J.S. Luterbacher, D.M. Alonso, J.A. Dumesic, Solvent effects in acid-catalyzed biomass conversion reactions, Angew. Chem. Int. Ed. Engl. 53 (2014) 11872–11875.
[18] S.K.N.H. Md Dostagir, M.K. Awasthi, A. Kumar, K. Gupta, S. Behrens, A. Shrotri, S. K. Singh, Selective catalysis for room-temperature hydrogenation of biomass-derived compounds over supported NiPd catalysts in water, ACS Sustain. Chem. Eng. 7 (2019) 9352–9359.
[19] T. Varila, E. Mäkelä, R. Kupila, H. Romar, T. Hu, R. Karinen, R.L. Puurunen, U. Lassi, Conversion of furfural to 2-methylfuran over CuNi catalysts supported on biobased carbon foams, Catal. Today 367 (2021) 16–27.
[20] M.A. Golubeva, A.L. Maximov, Hydroprocessing of furfural over in situ generated nickel phosphide based catalysts in different solvents, Appl. Catal. A: Gen. 608 (2020), 117890.
[21] K. Fulajtárova, T. Soták, M. Hronec, I. Vávra, E. Dobročka, M. Omastová, Aqueous phase hydrogenation of furfural to furfuryl alcohol over Pd–Cu catalysts, Appl. Catal. A: Gen. 502 (2015) 78–85.
[22] M. Hronec, K. Fulajtárová, I. Vávra, T. Soták, E. Dobročka, M. Mičušík, Carbon supported Pd–Cu catalysts for highly selective rearrangement of furfural to cyclopentanone, Appl. Catal. B: Environ. 181 (2016) 210–219.
[23] J. Wu, G. Gao, J. Li, P. Sun, X. Long, F. Li, Efficient and versatile CuNi alloy nanocatalysts for the highly selective hydrogenation of furfural, Appl. Catal. B: Environ. 203 (2017) 227–236.
[24] S. Thongratkaew, C. Luadthong, S. Kiatphuengporn, P. Khemthong, P. Hirunsit, K. Faungnawakij, Cu-Al spinel-oxide catalysts for selective hydrogenation of furfural to furfuryl alcohol, Catal. Today 367 (2021) 177–188.
[25] T. Komanoya, T. Kinemura, Y. Kita, K. Kamata, M. Hara, Electronic effect of ruthenium nanoparticles on efficient reductive amination of carbonyl compounds, J. Am. Chem. Soc. 139 (2017) 11493–11499.

[26] G. Liang, J. Zhao, A. Khodakov, V. Ordomsky, Structure-sensitive and insensitive reactions in alcohol amination over non-supported Ru nanoparticles, ACS Catal. 8 (12) (2018) 11226–11234.

[27] Q. Yuan, D. Zhang, L. van Haandel, F. Ye, T. Xue, E.J. Hensen, Y. Guan, Selective liquid phase hydrogenation of furfural to furfuryl alcohol by Ru/Zr-MOFs, J. Mol. Catal. A: Chem. 406 (2015) 58–64.

[28] J. Yang, J. Ma, Q. Yuan, P. Zhang, Y. Guan, Selective hydrogenation of furfural on Ru/Al-MIL-53: a comparative study on the effect of aromatic and aliphatic organic linkers, RSC Adv. 6 (2016) 92299–92304.

[29] J.J. Musci, A.B. Merlo, M.L. Casella, Aqueous phase hydrogenation of furfural using carbon-supported Ru and RuSn catalysts, Catal. Today 296 (2017) 43–50.

[30] J. Lee, J. Woo, C. Nguyen-Huy, M.S. Lee, S.H. Joo, K. An, Highly dispersed Pd catalysts supported on various carbons for furfural hydrogenation, Catal. Today 350 (2020) 71–79.

[31] D. Wu, W.Y. Hernández, S. Zhang, E.I. Vovk, X. Zhou, Y. Yang, A.Y. Khodakov, V. V. Ordomsky, In Situ Generation of Brønsted Acidity in the Pd-I Bifunctional Catalysts for Selective Reductive Etherification of Carbonyl Compounds under Mild Conditions, ACS Catalysis 9 (4) (2019) 2940–2948.

[32] J. Lee, J. Woo, C. Nguyen-Huy, M.S. Lee, S.H. Joo, K. An, Highly dispersed Pd catalysts supported on various carbons for furfural hydrogenation, Catal. Today 350 (2020) 71–79.

[33] Q. Fang, Z. Jiang, K. Guo, X. Liu, Z. Li, G. Li, C. Hu, Low temperature catalytic conversion of oligomers derived from lignin in pubescens on Pd/NbOPO4, Applied Catalysis B: Environmental 263 (2020), 128103.

[34] X. Kong, Y. Zhu, Z. Fang, J.A. Kozinski, I.S. Butler, L. Xu, H. Song, X. Wei, Catalytic conversion of 5-hydroxymethylfurfural to some value-added derivatives, Green Chem. 20 (2018) 3657–3682.

[35] M.J. Taylor, S.K. Beaumont, M.J. Islam, S. Tsatsos, C.A. Parlett, M.A. Issacs, G. Kyriakou, Atom efficient PtCu bimetallic catalysts and ultra dilute alloys for the selective hydrogenation of furfural, Appl. Catal. B: Environ. 284 (2021), 119737.

[36] B. Zhu, C. Chen, L. Huai, Z. Zhou, L. Wang, J. Zhang, 2, 5-Bis (hydroxymethyl) furan: a new alternative to HMF for simultaneously electrocatalytic production of FDCA and H2 over CoOOH/Ni electrodes, Appl. Catal. B: Environ. 297 (2021), 120396.

[37] R.M. Mironenko, O.B. Belskaya, T.I. Gulyaeva, A.I. Nizovskii, A.V. Kalinkin, V. I. Bukhtiyarov, A.V. Lavrenov, V.A. Likholobov, Effect of the nature of carbon support on the formation of active sites in Pd/C and Ru/C catalysts for hydrogenation of furfural, Catal. Today 249 (2015) 145–152.

[38] C. Ramirez-Barria, M. Isaacs, K. Wilson, A. Guerrero-Ruiz, I. Rodríguez-Ramos, Optimization of ruthenium based catalysts for the aqueous phase hydrogenation of furfural to furfuryl alcohol, Appl. Catal. A: Gen. 563 (2018) 177–184.

[39] J. Chen, F. Lu, J. Zhang, W. Yu, F. Wang, J. Gao, J. Xu, Immobilized Ru clusters in nanosized mesoporous zirconium silica for the aqueous hydrogenation of furan derivatives at room temperature, ChemCatChem 5 (2013) 2822–2826.

[40] X.-F. Yang, A. Wang, B. Qiao, J. Li, J. Liu, T. Zhang, Single-atom catalysts: a new frontier in heterogeneous catalysis, Acc. Chem. Res. 46 (2013) 1740–1748.

[41] G. Giorgianni, S. Abate, G. Centi, S. Perathoner, S. van Beuzekom, S.-H. Soo-Tang, J.C. Van der Waal, Effect of the solvent in enhancing the selectivity to furan derivatives in the catalytic hydrogenation of furfural, ACS Sustain. Chem. Eng. 6 (2018) 16235–16247.

[42] H. Struebing, Z. Ganase, P.G. Karamertzanis, E. Siougkrou, P. Haycock, P. M. Piccione, A. Armstrong, A. Galindo, C.S. Adjiman, Computer-aided molecular design of solvents for accelerated reaction kinetics, Nat. Chem. 5 (2013) 952–957.

[43] A. Cadu, K. Sekine, J. Mormul, D.M. Ohlmann, T. Schaub, A.S.K. Hashmi, Homogeneous catalysed hydrogenation of HMF, Green Chem. 20 (2018) 3386–3393.

[44] C. Copéret, A. Comas-Vives, M.P. Conley, D.P. Estes, A. Fedorov, V. Mougel, H. Nagae, F. Núñez-Zarur, P.A. Zhizhko, Surface organometallic and coordination chemistry toward single-site heterogeneous catalysts: strategies, methods, structures, and activities, Chem. Rev. 116 (2016) 323–421.

[45] Y. Deng, R. Gao, L. Lin, T. Liu, X.D. Wen, S. Wang, D. Ma, Solvent tunes the selectivity of hydrogenation reaction over alpha-MoC catalyst, J. Am. Chem. Soc. 140 (2018) 14481–14489.

[46] X. He, Q. He, Y. Deng, M. Peng, H. Chen, Y. Zhang, S. Yao, M. Zhang, D. Xiao, D. Ma, B. Ge, H. Ji, A versatile route to fabricate single atom catalysts with high chemoselectivity and regioselectivity in hydrogenation, Nat. Commun. 10 (2019) 3663.

[47] X. Chen, L. Zhang, B. Zhang, X. Guo, X. Mu, Highly selective hydrogenation of furfural to furfuryl alcohol over Pt nanoparticles supported on g-C_3N_4 nanosheets catalysts in water, Sci. Rep. 6 (2016) 28558.

[48] S. Tian, Z. Wang, W. Gong, W. Chen, Q. Feng, Q. Xu, C. Chen, C. Chen, Q. Peng, L. Gu, H. Zhao, P. Hu, D. Wang, Y. Li, Temperature-Controlled selectivity of hydrogenation and hydrodeoxygenation in the conversion of biomass molecule by the Ru1/mpg-C_3N_4 catalyst, J. Am. Chem. Soc. 140 (2018) 11161–11164.

[49] Q. Wang, S. Santos, C.A. Urbino-Blanco, W.Y. Hernández, M. Impéror-Clerc, E. I. Vovk, M. Marinova, O. Ersen, W. Baaziz, O.V. Safonova, A.Y. Khodakov, M. Saeys, V.V. Ordomsky, Solid micellar Ru single-atom catalysts for the water-free hydrogenation of CO2 to formic acid, Applied Catalysis B: Environmental 290 (2021) 120036.

[50] G. Li, B. Wang, B. Chen, D.E. Resasco, Role of water in cyclopentanone self-condensation reaction catalyzed by MCM-41 functionalized with sulfonic acid groups, J. Catal. 377 (2019) 245–254.

[51] M.J. Frisch, G.W. Trucks, H.B. Schlegel, G.E. Scuseria, M.A. Robb, J.R. Cheeseman, G. Scalmani, V. Barone, G.A. Petersson, H. Nakatsuji, X. Li, M. Caricato, A.V. Marenich, J. Bloino, B.G. Janesko, R. Gomperts, B. Mennucci, H.P. Hratchian, J.V. Ortiz, A.F. Izmaylov, J.L. Sonnenberg, Williams, F. Ding, F. Lipparini, F. Egidi, J. Goings, B. Peng, A. Petrone, T. Henderson, D. Ranasinghe, V.G. Zakrzewski, J. Gao, N. Rega, G. Zheng, W. Liang, M. Hada, M. Ehara, K. Toyota, R. Fukuda, J. Hasegawa, M. Ishida, T. Nakajima, Y. Honda, O. Kitao, H. Nakai, T. Vreven, K. Throssell, J.A. Montgomery Jr., J.E. Peralta, F. Ogliaro, M.J. Bearpark, J.J. Heyd, E.N. Brothers, K.N. Kudin, V.N. Staroverov, T.A. Keith, R. Kobayashi, J. Normand, K. Raghavachari, A.P. Rendell, J.C. Burant, S.S. Iyengar, J. Tomasi, M. Cossi, J.M. Millam, M. Klene, C. Adamo, R. Cammi, J.W. Ochterski, R.L. Martin, K. Morokuma, O. Farkas, J.B. Foresman, D.J. Fox, Gaussian 16 Rev. C.01, Wallingford, CT, 2016.

[52] C. Adamo, V. Barone, Toward reliable density functional methods without adjustable parameters: the PBE0 model, J. Chem. Phys. 110 (1999) 6158–6170.

[53] S. Grimme, S. Ehrlich, L. Goerigk, Effect of the damping function in dispersion corrected density functional theory, J. Comput. Chem. 32 (2011) 1456–1465.

[54] F. Weigend, R. Ahlrichs, Balanced basis sets of split valence, triple zeta valence and quadruple zeta valence quality for H to Rn: design and assessment of accuracy, Phys. Chem. Chem. Phys. 7 (2005) 3297–3305.

[55] X. Liu, W.-C. Lu, C.Z. Wang, K.M. Ho, Energetic and fragmentation stability of water clusters (H2O)n, n=2–30, Chem. Phys. Lett. 508 (2011) 270–275.

[56] D. Wu, Q. Wang, O.V. Safonova, D.V. Peron, W. Zhou, Z. Yan, M. Marinova, A. Y. Khodakov, V.V. Ordomsky, Lignin compounds to monoaromatics: selective cleavage of C– O bonds over a brominated ruthenium catalyst, Angew. Chem. 133 (2021) 12621–12631.

[57] S.Y. Chin, C.T. Williams, M.D. Amiridis, FTIR studies of CO adsorption on Al_2O_3- and SiO_2-supported Ru catalysts, J. Phys. Chem. B 110 (2006) 871–882.

[58] R. Breslow, Hydrophobic effects on simple organic reactions in water, Acc. Chem. Res. 24 (1991) 159–164.

[59] M.F. Neira D'Angelo, V. Ordomsky, J. van der Schaaf, J.C. Schouten, T.A. Nijhuis, Aqueous phase reforming in a microchannel reactor: the effect of mass transfer on hydrogen selectivity, Catal. Sci. Technol. 3 (2013) 2834–2842.

[60] P.G.D. Nicolas Giovambattista, Peter J. Rossky, Effect of surface polarity on water contact angle and interfacial hydration structure, J. Phys. Chem. B 111 (2007).

[61] W.J. Zhou, L. Fang, Z. Fan, B. Albela, L. Bonneviot, F. De Campo, M. Pera-Titus, J. M. Clacens, Tunable catalysts for solvent-free biphasic systems: pickering interfacial catalysts over amphiphilic silica nanoparticles, J. Am. Chem. Soc. 136 (2014) 4869–4872.

[62] J.P. Guthrie, Hydration of carbonyl compounds, an analysis in terms of multidimensional marcus theory, J. Am. Chem. Soc. 122 (2000) 5529–5538.

[63] H.J. Buschmann, H.H. Füldner, W. Knoche, The reversible hydration of carbonyl compounds in aqueous solution. Part I, the keto/gem-diol equilibrium, Ber. der Bunsenges. für Phys. Chem. 84 (1980) 41–44.

[64] Y. Yang, D. Rao, Y. Chen, S. Dong, B. Wang, X. Zhang, M. Wei, Selective Hydrogenation of Cinnamaldehyde over Co-Based Intermetallic Compounds Derived from Layered Double Hydroxides, ACS Catal. 8 (2018) 11749–11760.

[65] B. Coq, P. Kumbhar, C. Moreau, P. Moreau, M.J.J.o.M.C. Warawdekar, Liquid Phase Hydrogenation of Cinnamaldehyde Over Supported Ruthenium Catalysts: Influence of Particle Size, Bimetallics and Nature of Support, 85 (1993) 215–228.

[66] F.J. Feher, D.A. Newman, J.F. Walzer, Silsesquioxanes as models for silica surfaces, J. Am. Chem. Soc. 111 (1989) 1741–1748.

[67] P.J. Dyson, P.G. Jessop, Solvent effects in catalysis: rational improvements of catalysts via manipulation of solvent interactions, Catal. Sci. Technol. 6 (2016) 3302–3316.

[68] M.J. Kamlet, J.L.M. Abboud, M.H. Abraham, R.W. Taft, Linear solvation energy relationships. 23. A comprehensive collection of the solvatochromic parameters,. pi.*,.alpha., and.beta., and some methods for simplifying the generalized solvatochromic equation, J. Org. Chem. 48 (1983) 2877–2887.

[69] W.-H. Wang, J.T. Muckerman, E. Fujita, Y. Himeda, Mechanistic insight through factors controlling effective hydrogenation of CO_2 catalyzed by bioinspired proton-responsive iridium(III) complexes, ACS Catal. 3 (2013) 856–860.